A. Benallal, G. Cailletaud,† J. L. Chaboche,‡ D. Marquis,* D. Nouailhas,‡ and M. Rousset†*

Description and Modelling of Non-Proportional Effects in Cyclic Plasticity

REFERENCE Benallal, A., Cailletaud, G., Chaboche, J. L., Marquis, D., Nouailhas, D., and Rousset, M., **Description and modelling of non-proportional effects in cyclic plasticity,** *Biaxial and Multiaxial Fatigue*, EGF 3 (Edited by M. W. Brown and K. J. Miller), 1989, Mechanical Engineering Publications, London, pp. 107–129.

ABSTRACT This paper is concerned with the behaviour of materials under nonproportional loading. Basic features of this behaviour are described and include:

(a) supplementary hardening with respect to proportional loading;
(b) recovery of this hardening when decreasing the nonproportionality of the loading;
(c) a cross-hardening effect.

It is then shown that classical formulations of plasticity are inadequate to describe these effects. Two modifications of these formulations are therefore proposed in order to take into account the non-proportionality of the loading. Numerical simulations of very complex tests are given to show the improvements which can be achieved by these modifications.

Introduction

Investigations into the mechanisms of single crystal hardening at a micro-structural scale allow one to define several types of interaction occurring during plastic straining, either between the dislocations themselves (intersection processes), or between the dislocations and the lattice structure (PEIERLS force). A number of studies have dealt with FCC structures (Cu, Al) and the most popular experiment is the latent hardening test, during which a single crystal specimen is axially loaded in a given direction, then machined and loaded again along a second orientation (**1**)(**2**). Generally, with this procedure, two different slip systems are activated successively. The interpretation uses the concept of a latent hardening ratio (LHR), that is the ratio of the critical resolved shear stress on the second activated system to the critical resolved shear stress reached at the first level: hence, LHR is a measurement of the latent hardening (or cross hardening) induced on the second system by the straining of the first. The experimental curves of LHR show an anisotropy of this hardening. Further, the latent hardening is found to be higher than the self hardening, that is the strengthening of the first system induced by its own strain.

* Laboratoire de Mecanique et Technologie, ENS de Cachan/CNRS/Universite Paris 6, 61, avenue du Président Wilson-94230 Cachan.
† Centre des Materiaux de l'Ecole des Mines de Paris, BP87-91003 EVRY cedex
‡ ONERA Division ORRF, 29 avenue de la Division Lecterc-92320 Chatillon sous Bagneux.

The maximum values of LHR reached in copper for small strains (less than 1 per cent) (**3**) are within the range 1.5–4.00.

The modelling of this latent hardening has also received the authors' attention. The commonly used phenomenological hardening law at a microstructural level is the hardening matrix, relating in a crystal the critical resolved shear stress rate with the plastic shear strain rate of all the slip systems (**4**).

$$\dot{\tau}_c = \mathbf{H}\dot{\gamma}^p \tag{1}$$

The dimension of the vectors τ_c and γ^p is equal to the number of slip systems in the crystal; the square matrix **H** is built with its diagonal terms describing self hardening and with the off-diagonal ones describing cross hardening.

The action of latent hardening has been recently exhibited by more complex tests (**5**)–(**11**). During these tests, cyclic loading involving multiaxial complex straining paths are applied to polycrystals. As in the case of the classical test on single crystals, the change of the loading direction is found to induce an additional hardening. A detailed description of the experimentally observed phenomena is given later in this paper.

Of course, more developments (specially for the hardening rules) are required to apply slip system theory to polycrystals, but this type of model is not available for computations at the present time. On the other hand, the classical models of plasticity or viscoplasticity using a macroscopic yield surface (von Mises' or Hill's criteria) are not adequate for the description of these phenomena (**12**), so we propose two ways of modifying these equations (distortion or isotropic change of the yield surface during non-proportional straining), to provide a better account for the supplementary hardening (SH) observed.

Notation

τ_c	Critical resolved shear stress
$\mathbf{H}$	Hardening matrix
γ^p	Plastic shear strain
$\bar{\sigma}$	von Mises' equivalent stress
σ	Stress tensor
$\bar{\sigma}_M$	Maximum equivalent stress
$\underline{s}$	Deviatoric stress tensor
ε^p	Equivalent plastic strain
$\underline{\varepsilon^p}$	Plastic strain tensor
ε_M^p	Maximum equivalent plastic strain
δ	Kronecker's symbol
$\varepsilon, \varepsilon_a$	Axial strain, axial strain amplitude
γ, γ_a	Shear strain, shear strain amplitude
ω	Angular frequency
φ	Phase lag between shear and axial strains
ϱ	Strain range ratio, $\gamma/\sqrt{3}\varepsilon$

φ^*	Phase lag between shear and axial stresses
ϱ^*	Stress range ratio, $\tau\sqrt{3}/\sigma$
X	Kinematic hardening variable or back stress tensor
R	Isotropic hardening variable or drag stress
Ω	Viscoplastic potential
J	Second invariant of active stress tensor $(s - X)$
$\dot{p}$	Rate of accumulated plastic strain
M	Anisotropy tensor
β	Rotation of the yield surface
A	Non-proportionality variable
α	Deviatoric stress rate and plastic strain rate angle
Q	Steady state value of drag stress, R
k	Initial yield stress
$K, n, c, a, b, Q_0, Q_{00}, g, d, f, Z, \phi_{00}, \bar{\omega}$	Material dependent parameters

Experimental results for non-proportional loading

The material chosen for this study is type 316 stainless steel. Thin-walled tubular axial–torsional specimens are machined from bars. The heat treatment of these bars involves soaking at 1050°C for one hour followed by a quench in water. All the tests are carried out on a strain-controlled tension–torsion servohydraulic system. Axial and shear strains are measured by strain gauges fixed on the cylindrical part of the specimen. All the tests are performed at room temperature and the equivalent strain rate lies between 2.10^{-4} s^{-1} and 3.10^{-3} s^{-1}.

Cyclic hardening

The behaviour of metallic materials under cyclic loading is characterized by the cyclic hardening curve. For viscoplastic materials, this curve is defined for a given value of the inelastic strain rate. Uniaxial and proportional strainings lead to the same cyclic curve if the von Mises' equivalent stress, $\bar{\sigma}$, and von Mises' equivalent plastic strain, $\overline{\varepsilon^p}$, are used.

$$\bar{\sigma} = \sqrt{\left(\frac{3}{2} S_{ij} S_{ij}\right)} \tag{2}$$

$$\overline{\varepsilon^p} = \sqrt{\left(\frac{2}{3} \varepsilon^p_{ij} \varepsilon^p_{ij}\right)} \tag{3}$$

$$S_{ij} = \sigma_{ij} - \frac{1}{3} \sigma_{kk} \delta_{ij} \tag{4}$$

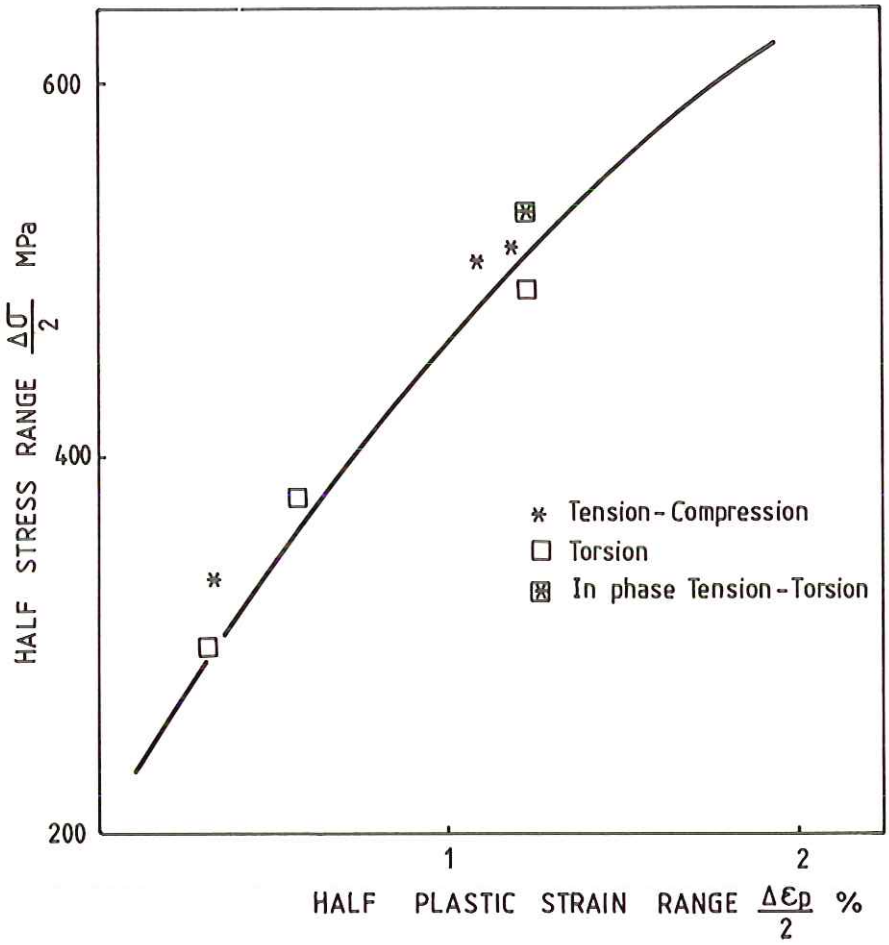

Fig 1 Cyclic equivalent stress strain curve under proportional loading for 316 stainless steel

In Fig. 1 are plotted the steady state results for different directions of straining.

Under non-proportional loading, cyclic hardening is stronger. As a matter of fact, a fully cyclically hardened specimen under proportional straining exhibits a supplementary strengthening for subsequent non-proportional loading with the same equivalent strain; see Fig. 2. The new steady state is reached after about 20 cycles. This hardening is compared to that obtained under in-phase loading by plotting the maximum equivalent stress versus the maximum equivalent plastic strain for the steady state (these two maxima are generally not obtained at the same time). Figure 3(a) and Table 1 present the experimental results obtained for different strain paths. For sinusoïdal out-of-phase

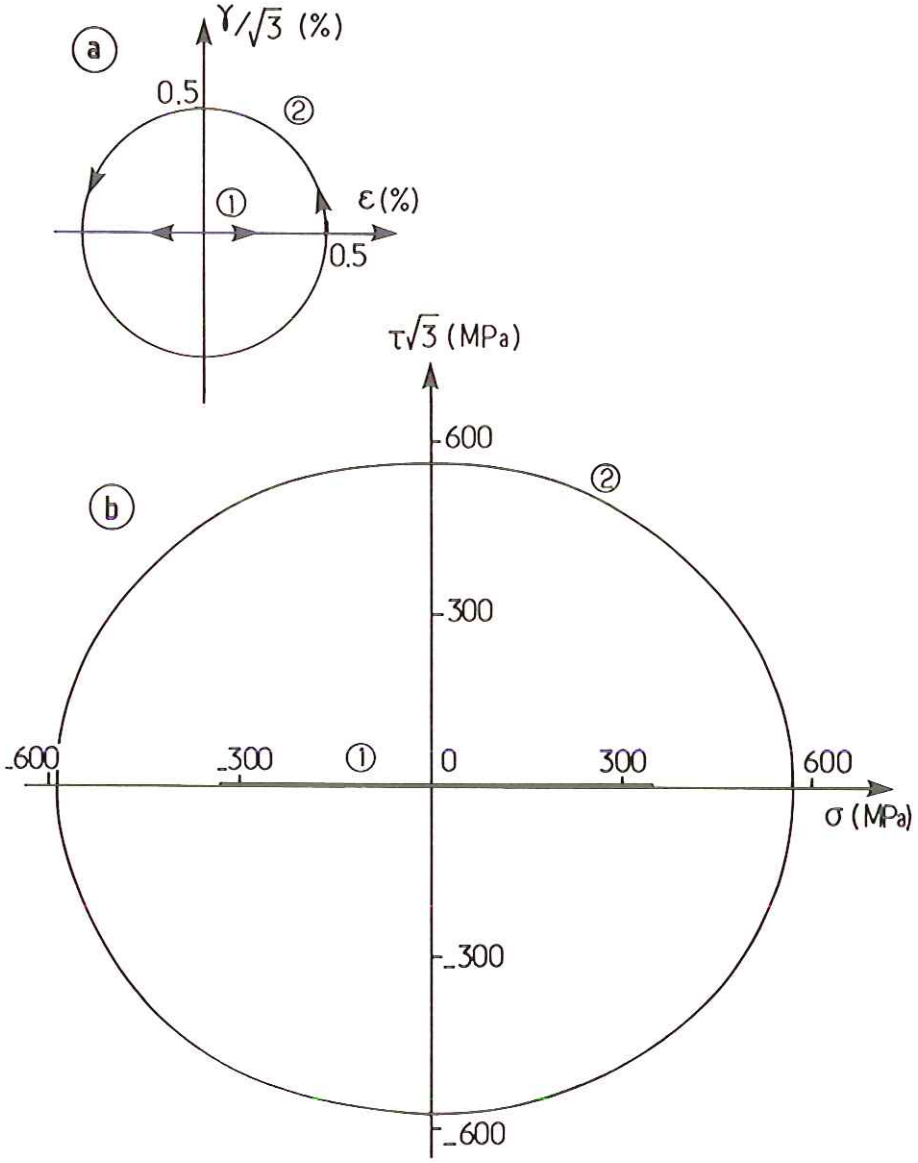

Fig 2 Non-proportional loading (2) subsequent to proportional loading (1): (a) straining paths, $\Delta\varepsilon = 1$ per cent, (b) steady state stress response

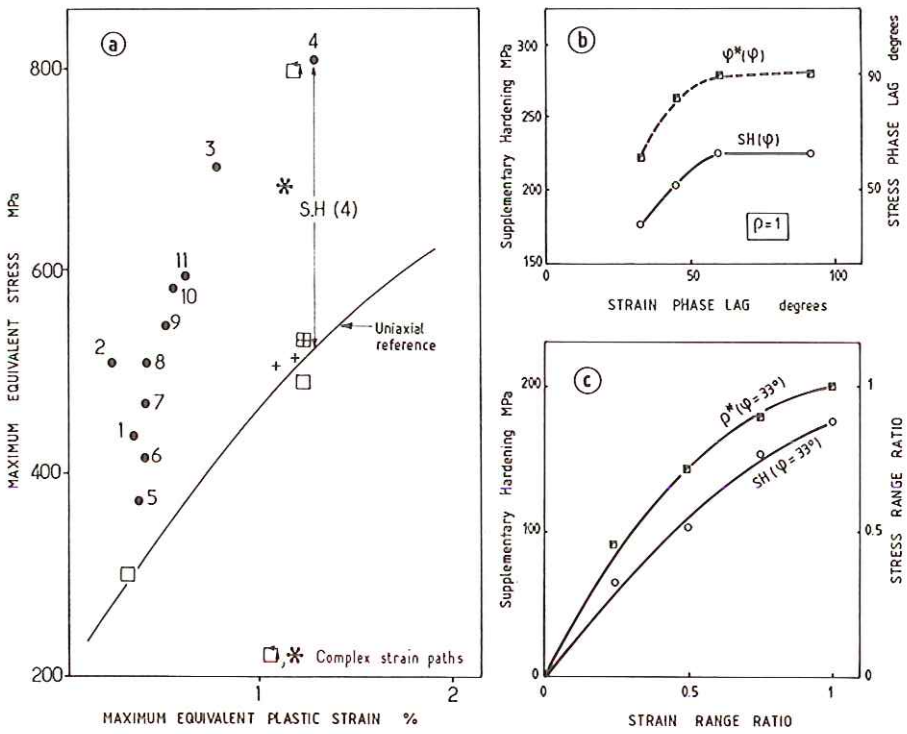

Fig 3 Influence of the degree of nonproportionality on supplementary hardening: (a) experimental results (see also Table 2), (b) effect of phase lag for a given strain range ratio, (c) effect of strain range ratio for a given phase lag

Table 1 Non-proportional loadings

	φ (degrees)	ϱ	φ^* (degrees)	$\varrho = \frac{\sqrt{3}\tau_{max}}{\sigma_{max}}$
1	−68	0.31	−90	0.85
2	−68	0.83	−90	0.99
3	−68	0.91	−90	1.07
4	−68	0.96	−90	0.98
5	33	0.25	67	0.46
6	33	0.5	66	0.67
7	33	0.66	69	0.83
8	33	1	69	0.92
9	45	1	82	0.99
10	60	1	90	1
11	92	1	90	1

paths, the loading parameters are the phase angle of lag φ and the strain range ratio ϱ

$$\varepsilon = \varepsilon_a \sin \omega t \tag{5}$$

$$\gamma = \gamma_a \sin (\omega t - \varphi) \tag{6}$$

$$\varrho = \gamma_a/\sqrt{3}\varepsilon_a \tag{7}$$

The main features of these results can be summarized as follows.

(i) For a given value of φ the greater the ratio ϱ, the stronger the supplementary hardening (SH); see Fig. 3(c). The value of SH is defined as the difference between the maximum equivalent stress and the equivalent stress given by the cyclic curve for the same equivalent plastic strain. A good correlation is obtained between the SH and the stress range ratio, ϱ^* $(= \sqrt{3}\tau_a/\sigma_a)$.

(ii) For a value of $\varrho = 1$, variations of φ between 30 and 90 degrees have little influence on the supplementary hardening; see Fig. 3(b). In this case, also, a good correlation is found between the SH and the phase lag φ^* between σ and τ.

(iii) Two complex strain paths (see Fig. 3(a)) are studied, and the SH varies between the cyclic curve ($\varphi = 0$) and the maximum value obtained under out-of-phase loading. Other complex paths have been reported and lead to the same conclusion (**13**).

Subsequent cyclic softening

The SH due to the non-proportionality of the loading is transitory. This effect is observed when, after an out-of-phase loading ($\varrho = 1$, $\varphi = 90$ degrees, $\bar{\varepsilon} = 0.53$ per cent), the specimen is subjected to cyclic tension loading ($\bar{\varepsilon}_M = 0.53$ per cent); see Fig. 4. The softening rate is very slow with respect to the previous hardening rate. After eighty cycles the stress range (960 MPa) is still higher than the one obtained under direct proportional straining (640 MPa).

Cross hardening effect

This effect appears when, after proportional straining in a given direction, the subsequent loading is proportional straining in another direction. For the same equivalent strain range, a change of the loading direction leads to a strengthening during the first subsequent cycles. This SH is followed by a slow softening; see Fig. 5(a). This behaviour is observed for the following paths.

(i) Cyclic tension up to the steady state, followed by cyclic torsion; see Fig. 5(b), Test 1, or the opposite sequence test 2.

(ii) Cyclic in-phase tension–torsion ($\varrho = 1$ and $\varphi = 0$) up to the steady state

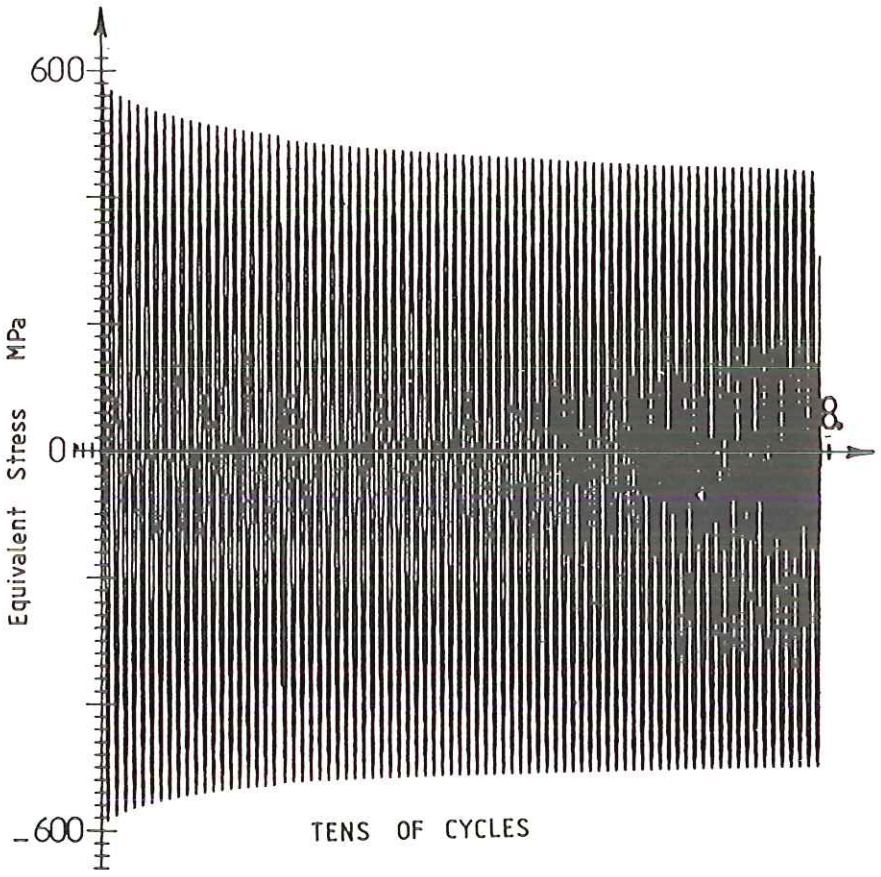

Fig 4 Subsequent cyclic softening under tension-compression loading, after out-of-phase loading ($\rho = 1$, $\varphi = 90$ degrees)

followed by the same type of loading with $\varrho = 1$ and $\varphi = 180$ degrees; see Fig. 5(a).

(iii) Repetition of the sequence of ten cycles in tension followed by ten cycles in torsion. The cross hardening effect is present after each change of loading direction; see Fig. 5(b), test 3.

The softening in test 2 is almost complete. In test 3 the SH is found to be permanent because the hardening rate is higher than the softening one. The cross hardening effect can be interpreted as a combination of SH induced by the non-proportionality of the loading at the change of the straining direction, and the softening induced by the subsequent proportional loading. The SH obtained in cross hardening tests is lower than in out-of-phase tests with the same equivalent strain; test 4, $\varrho = 1$, $\varphi = 90$ degrees.

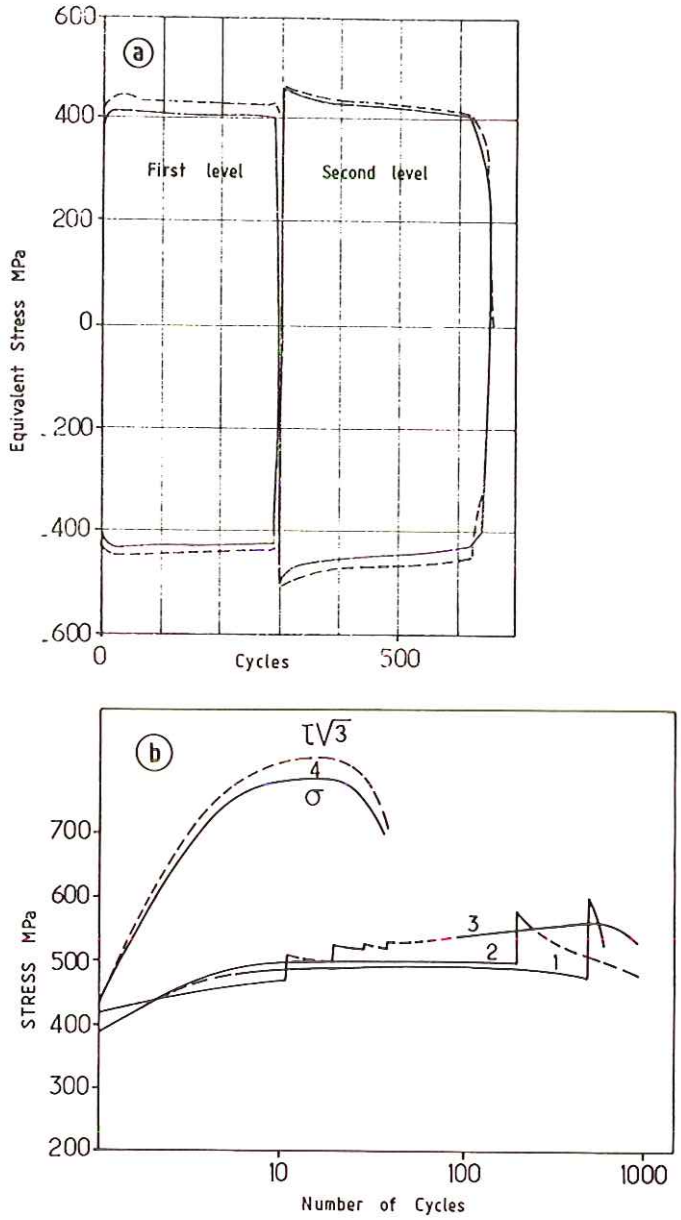

Fig 5 Cross hardening effects: (a) Maximum and minimum stresses (— σ_M and ···· $\tau_M\sqrt{3}$) for in-phase tension–torsion loading: first level $\rho = 1$, $\varphi = 0$ degrees; second level $\rho = 1$, $\varphi = 180$ degrees, (b) evolution of maximum equivalent stresses for different loading paths with the same equivalent strain ($\varepsilon = 3.1$ per cent)

Modelling

The classical formulation of plasticity or viscoplasticity based on the concept of internal variables and identified in proportional test results does not take into account the effects previously described. Two ways of modification are now proposed.

Classical formulation of elasto-viscoplasticity

Monotonic and cyclic behaviour of type 316 stainless steel at room temperature can be modelled successfully for proportional loading by introducing a non linear kinematic hardening rule. Plastic and creep strains are unified so that

$$\varepsilon_{ij} = \varepsilon^e_{ij} + \varepsilon^p_{ij} \tag{8}$$

The viscoplastic flow rate derives from a potential Ω. Equipotential surfaces are similar to the elastic domain. The size of the elastic domain is given by R (isotropic hardening) and its centre by X (kinematic hardening variable). The term k describes the initial yield stress.
Elastic domain

$$f = J(\sigma - X) - R - k < 0 \tag{9}$$

Viscoplastic potential

$$\Omega = \frac{K}{n+1}\left\langle \frac{f}{K} \right\rangle^{n+1} \tag{10}$$

Flow rule

$$\dot{\varepsilon}^p_{ij} = \frac{\partial \Omega}{\partial \sigma_{ij}} = \frac{3}{2}\left\langle \frac{f}{K} \right\rangle^{n} \frac{S_{ij} - X_{ij}}{J(\sigma - X)} \tag{11}$$

with

$$J(\sigma - X) = \sqrt{\left\{\frac{3}{2}(S_{ij} - X_{ij})(S_{ij} - X_{ij})\right\}} \qquad \text{equivalent active stress} \tag{12}$$

$$\dot{X}_{ij} = c\left\{\frac{2}{3}a\dot{\varepsilon}^p_{ij} - \phi(p)X_{ij}\dot{p}\right\} \tag{13}$$

$$\phi(p) = \phi_{00} + (1 - \phi_{00})\exp(-\bar{\omega}p) \tag{14}$$

$$\dot{R} = b(Q - R)\dot{p} \tag{15}$$

$$\dot{p} = \sqrt{\left(\frac{2}{3}\dot{\varepsilon}^p_{ij}\dot{\varepsilon}^p_{ij}\right)} \qquad \text{rate of accumulated plastic strain} \tag{16}$$

$$\langle g \rangle = g \quad \text{if} \quad g \geq 0 \qquad \text{and} \quad \langle g \rangle = 0 \quad \text{if} \quad g < 0$$

and $n, K, c, a, b, k, Q, \phi_{00}, \bar{\omega}$ are material dependent parameters. This model represents the basic features of the viscoplastic behaviour. Some modifications

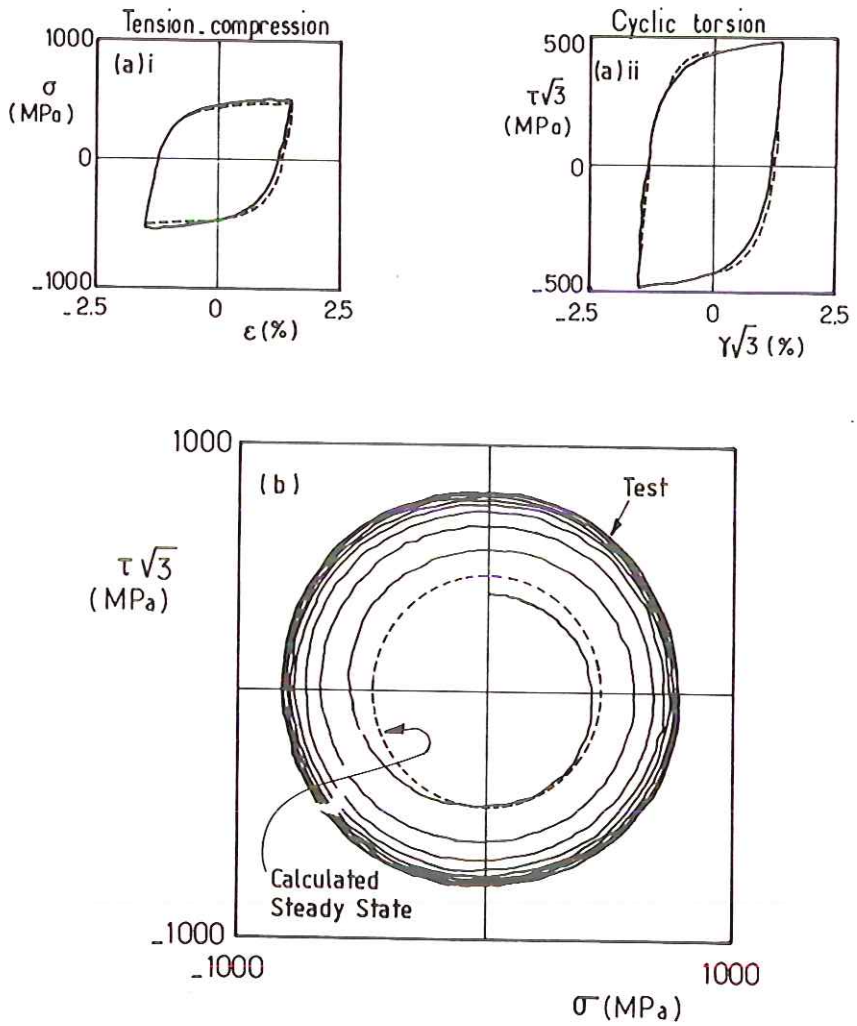

Fig 6 Steady states of proportional and nonproportional loading, — tests, ···· simulations: (a) proportional loading, (b) nonproportional loading ($\varphi = 0$ degrees; second level $\rho = 1$, $\varphi = 68$ degrees, $\rho = 0.96$, $\varepsilon_M = 3.1$ per cent)

have been made to describe the effect of the maximum plastic strain memory (**14**), the effect of the temperature history (**15**), and the time recovery effects (**16**), but the purpose of this paper is the description of nonproportional loading effects and in the investigated experimental domain, the previous effects are not predominant.

As a starting point to this study, a numerical simulation of nonproportional straining is made, using the basic model, previously identified in proportional tests. The illustration of both theory and experiment is shown in Fig. 6. The

prediction for proportional loading (tension–compression and cyclic torsion) is in good agreement with the experimental results (see Fig. 6(a)), but the predicted equivalent stress is lower than the experimental one for nonproportional loading; see Fig. 6(b). A modification of the hardening behaviour is then needed which means a modification of the yield surface in the presence of non-proportional loading. We first recall some characteristics of the results concerning the deformation of this surface.

Experimental study of elastic domains (**17**)

This study is made on 2024 aluminium alloy tubular specimens at room temperature. Cyclic tension–torsion tests are performed under proportional and non-proportional loading. Elastic domains are determined at different points of the loading path. To avoid the influence of elastic domain probing on the main cyclic loading, a plastic strain offset limited to $5 \cdot 10^{-5}$ is chosen. The good linearity of the elastic behaviour of the chosen material allows the use of such small offsets.

The main results obtained are as follows.

(i) *Distortion*. The distortion of the elastic domain is characterized by the formation, for a monotonic tensile test, of a smooth corner in the loading direction and a flat zone in the opposite one; see Fig. 7(a).

(ii) *Reverse distortion*. During an unloading, the elastic domain exhibits a new corner in the new direction of loading. The distortion is not memorized; see Fig. 7(b).

(iii) *Cross-effect*. The size (measured by Tresca's norm as the initial surface is very close to the ellipse given by the Tresca's criterion) of the elastic domain in the loading direction is smaller than the maximum size in the perpendicular direction. This is the mechanical illustration of the 'latent hardening' which basically explains the SH; see Figs 7(a) and (b).

(iv) *Cyclic expansion*. For nonproportional straining, the elastic domain suffers distortion, kinematic and strong isotropic hardening. For a rectangular strain path (see Fig. 8), the elastic domains determined at the same point (A) at successive cycles, have almost the same shape. The major difference from one cycle to the subsequent one is the expansion of the elastic domain. It can be noted also that the normality of the plastic strain rate to the elastic domain is well verified.

These observations suggest two ways of improvement of the classical models. The first one takes into account the distortion of the elastic domain. The second one modifies only the isotropic hardening rule.

Model 1: anisotropy of the elastic domain (**12**)

Formulation

The model used is an extension of the rule proposed by Baltov and Sawczuk

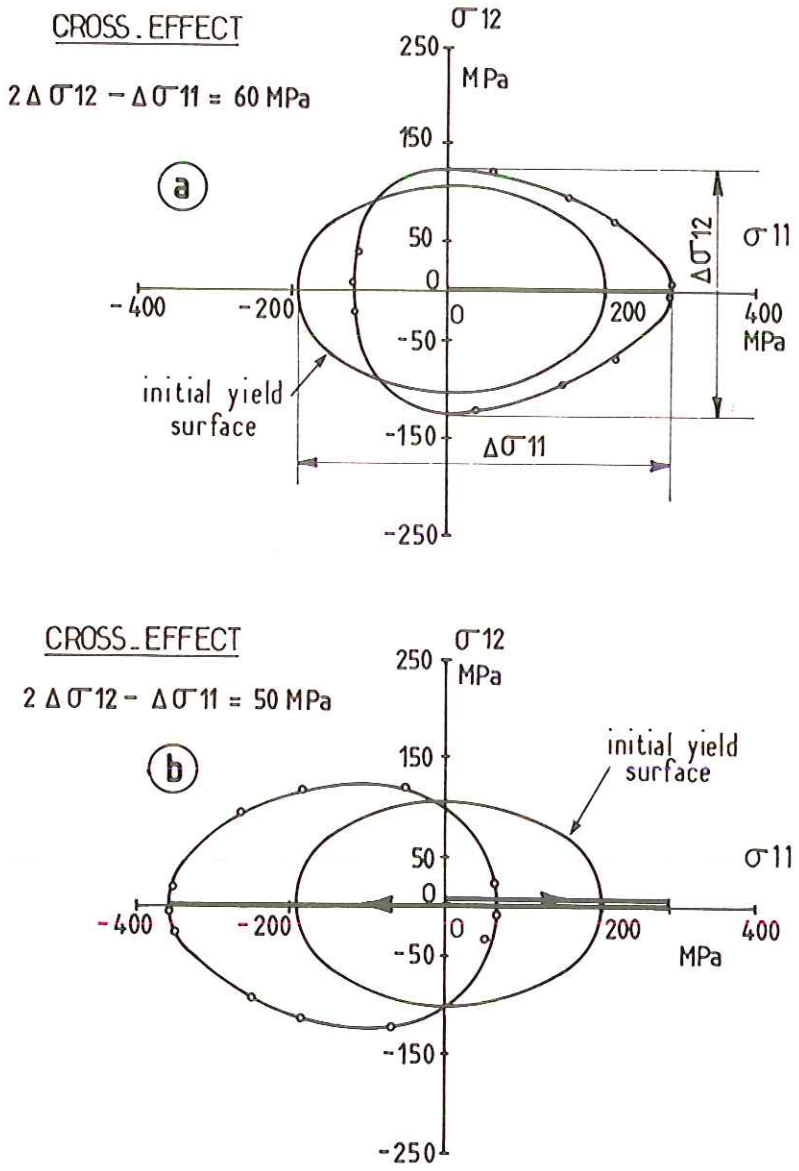

Fig 7 Distortion of the elastic domain of 2024 aluminium alloy: (a) monotonic tensile test up to 300 MPa ($\varepsilon^p = 1.5$ per cent), (b) reverse distortion in subsequent compression up to −360 MPa ($\varepsilon^p = 0$ per cent)

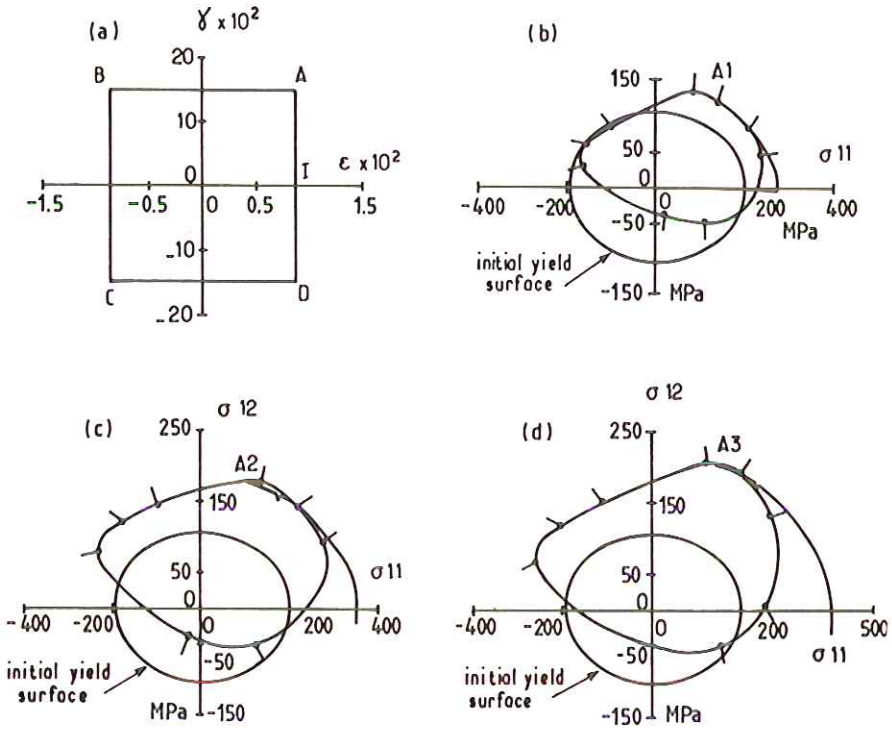

Fig 8 Elastic domain evolution in square strain path: (a) forced strain path: OIABCDABCDABCD, (b) elastic domain at point A for the first cycle, (c) elastic domain at point A for the second cycle, (d) elastic domain at point A for the third cycle. The segments reported on the figures give the plastic strain increments directions

(18). It models neither corners nor flat zones, but describes the cross effect. This effect can be considered as continuously present during out-of-phase loading. This rule is introduced in the context of viscoplasticity theory. Kinematic and isotropic hardening rules are those used in the classical formulation (equations (13) and (15)). Only the expression of the elastic domain (equation (9)) is modified by

$$f_a = \sqrt{\left\{\frac{3}{2}\frac{3\,M_{ijkl}}{(1+(3/2)Z\bar{\varepsilon}^{p2})}(S_{ij}-X_{ij})(S_{kl}-X_{kl})\right\}} - R - k < 0 \qquad (17)$$

The components of the fourth order tensor M_{ijk} are plastic strain dependent

$$M_{ijkl} = I_{ijkl} + Z\varepsilon^p_{ij}\varepsilon^p_{kl} \qquad (18)$$

with

$$I_{ijkl} = \frac{1}{2}\left(\delta_{ik}\delta_{jl} + \delta_{il}\delta_{jk} - \frac{2}{3}\delta_{ij}\delta_{kl}\right) \qquad (19)$$

The term Z is an anisotropy coefficient, which describes the expansion of the shrinking of the elastic domain. When $Z = 0$, this corresponds to the von Mises' criterion.

In addition to translation and expansion of the elastic domain, such a rule accounts for its rotation. The material is assumed to be initially isotropic. In the particular case of tension–torsion loading, the equation of the elastic domain in the plane $(\sigma, \tau\sqrt{3})$ becomes

$$f_a = \sqrt{\left[\frac{\{1 + (3/2)Z\varepsilon_{11}^{p2}\}(\sigma - X)^2 + 3Z\varepsilon_{11}^{p}\varepsilon_{12}^{p}(\sigma - X) \times (\tau - X_{12}) + 3(1 + 2Z\varepsilon_{12}^{p2})(\tau - X_{12})^2}{1 + (3/2)Z\varepsilon_{11}^{p2} + 2Z\varepsilon_{12}^{p2}}\right]} - R - k \leq 0 \quad (20)$$

with

$$X_{11} = \frac{2}{3}X$$

and

$$X_{22} = X_{33} = -\frac{X}{3}$$

The original surface deforms into an ellipse, with centre $(X, \sqrt{3}X_{12})$. It rotates through the angle β given by

$$\text{tg } 2\beta = \frac{\sqrt{3}\varepsilon_{11}^{p}\varepsilon_{12}^{p}}{(3/2)\varepsilon_{11}^{p2} - 2\varepsilon_{12}^{p2}} \quad (21)$$

The semi-axes of the ellipse are given by

$$b_0^2 = \frac{(2 + 3Z\varepsilon_{11}^{p2} + 4Z\varepsilon_{12}^{p2})(R + k)^2}{\{2 + (3/2)Z\varepsilon_{11}^{p2} + 2Z\varepsilon_{12}^{p2}\} - Z\sqrt{[\{(3/2)\varepsilon_{11}^{p2} - 2\varepsilon_{12}^{p2}\}^2 + 3\varepsilon_{11}^{p2}\varepsilon_{12}^{p2}]}} \quad (22)$$

$$a_0^2 = \frac{(2 + 3Z\varepsilon_{11}^{p2} + 4Z\varepsilon_{12}^{p2})(R + k)^2}{\{2 + (3/2)Z\varepsilon_{11}^{p2} + 2Z\varepsilon_{12}^{p2}\} + Z\sqrt{[\{(3/2)\varepsilon_{11}^{p2} - 2\varepsilon_{12}^{p2}\}^2 + 3\varepsilon_{11}^{p2}\varepsilon_{12}^{p2}]}} \quad (23)$$

With regard to the initial Baltov and Sawczuk model, the introduction of the term $\{1 + (3/2)Z\bar{\varepsilon}^{p2}\}$ in equation (17) is such that this model gives the same results as the classical formulation (equation (9)) for uniaxial tension or torsion. If the specimen is subjected to axial tension, the values of the semi-axes of the ellipse are defined by

$$\begin{aligned} a_0 &= R + k \\ b_0 &= (R + k)\sqrt{\{1 + (3/2)Z\varepsilon_{11}^{p2}\}} \end{aligned} \quad (24)$$

and for torsion, by

$$\begin{aligned} a_0 &= (R + k)\sqrt{(1 + 2Z\varepsilon_{12}^{p2})} \\ b_0 &= R + k \end{aligned} \quad (25)$$

It is clear from equation (19) that the elastic domain does not rotate for the two particular cases ($\varepsilon^p_{11} = 0$ or $\varepsilon^p_{12} = 0$). The cross-effect depends on the value of Z and the elastic domain expands more in the perpendicular direction to the loading if Z is positive.

The introduction of the anisotropy of the elastic domain in the viscoplastic formulation is done by modifying the viscoplastic potential, equation (10) to the form

$$\Omega = \frac{K}{n+1}\left\langle \frac{f_a}{K} \right\rangle^{n+1} \tag{26}$$

Characteristic results

From a quantitative point of view, this model can describe the major effect which is the supplementary hardening under out-of-phase loading, with only one more coefficient. For a given value of Z, the additional hardening increases with the plastic strain. A way to bound the SH for the large plastic strains is to use the components of the non-linear kinematic hardening variable instead of the plastic strain (**12**): in equation (17) $\overline{\varepsilon^p}$ is replaced by $\overline{X}$ with

$$\overline{X} = \sqrt{\left(\frac{1}{2} X_{ij} X_{ij}\right)} \tag{27}$$

On the other hand, the model does not describe the cross hardening effect because the anisotropy instantaneously disappears when the plastic strain takes a zero value. So, the subsequent softening is complete and instantaneous.

Model 2: Modification of the isotropic hardening rule (**11**)

In this part, we develop a second model with an elastic domain without distortion and isotropic hardening that depends upon an additional variable which takes into account the nonproportionality of the loading path.

Nonproportionality variable

In order to distinguish the proportional loading cases from the others, the angle between vectors representing the stress and the plastic strain, or the rates of these vectors can be introduced. Indeed, in the deviatoric plane, proportional loading is such that these angles are null, and for non-proportional loading they are different from zero; see Fig. 9.

In plasticity, the angle between s and ε^p lies between $-\pi/2$ and $\pi/2$. This angle is chosen to define the nonproportionality variable A as

$$A = 1 - \cos^2 \alpha = \sin^2 \alpha \tag{28}$$

where

$$\cos \alpha = \frac{\dot{\varepsilon}^p_{ij} \dot{s}_{ij}}{\sqrt{(\dot{\varepsilon}^p_{ij} \dot{\varepsilon}^p_{ij})}\sqrt{(\dot{s}_{ij} \dot{s}_{ij})}} \tag{29}$$

For proportional loading $A = 0$ and for non-proportional loading $0 < A \leq 1$.

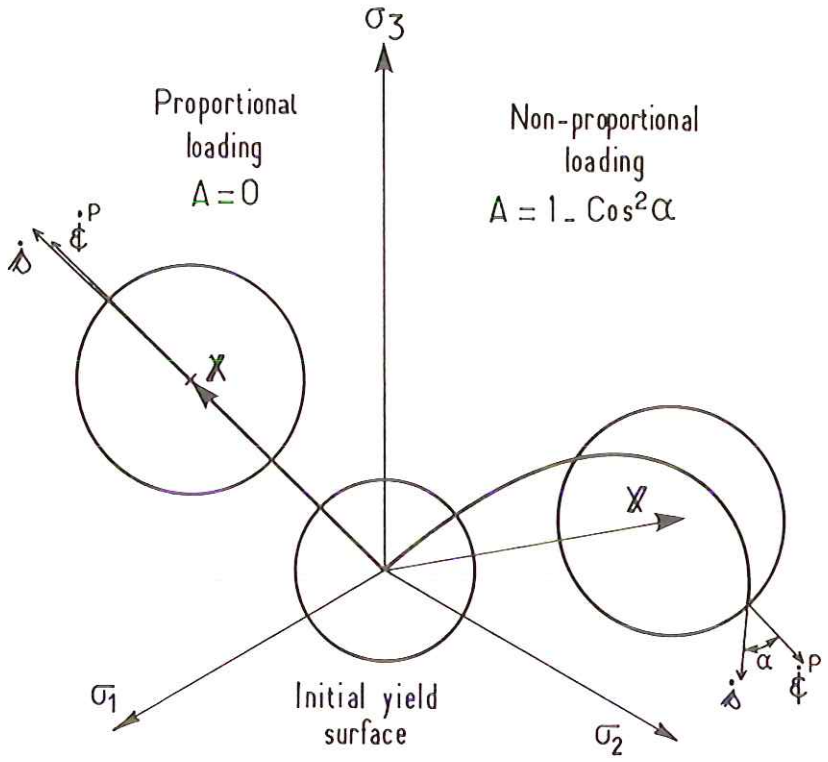

Fig 9 Definition of the non-proportionality variable

Modification of the isotropic hardening rule

The asymptotic value Q of R which represents the size of the yield surface is a constant in the classical formulation. Here Q is considered as a new variable. We assume that this variable is a strain hardening one. Its evolution law is

$$\dot{Q} = D(A)\{Q_{AS}(A) - Q\}\dot{p} \tag{30}$$

with

$$D(A) = (d - f)A + f \tag{31}$$

and

$$Q_{AS}(A) = \frac{gAQ_{00} + (1 - A)Q_0}{gA + (1 - A)} \tag{32}$$

Here d, f, g, Q_{00} and Q_0 are material dependent parameters. If $A = 0$, we have

$$\dot{Q} = f(Q_0 - Q)\dot{p} \tag{33}$$

and as the initial value of Q is Q_0, in proportional loading Q remains equal to

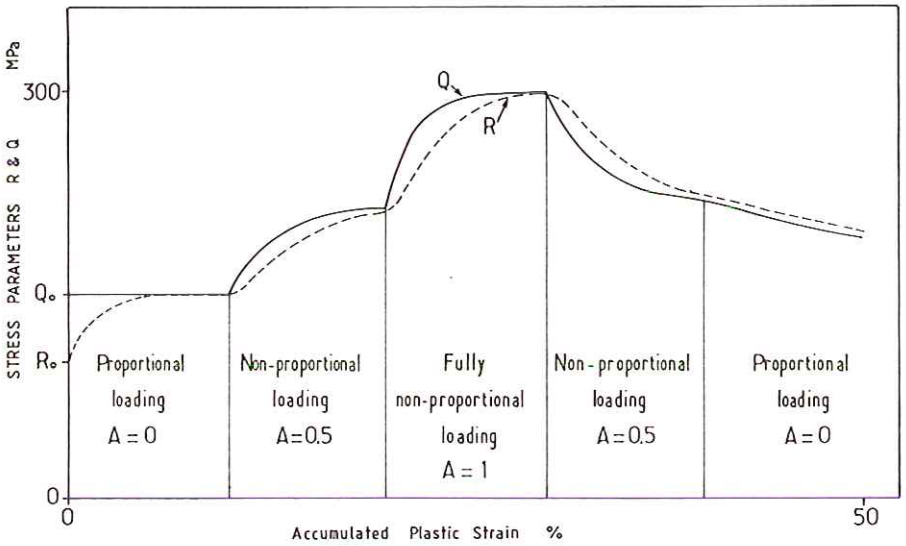

Fig 10 Evolution of the isotropic hardening variable in complex loading paths

Q_0 and the classical isotropic hardening law is retrieved; equation (15). If $A = 1$, equation (30) becomes

$$\dot{Q} = d(Q_{00} - Q)\dot{p} \tag{34}$$

and the strongest nonproportionality is obtained. The deviatoric stress rate is then tangent to a viscoplastic equipotential. The maximum supplementary hardening is $(Q_{00} - Q_0)$; Q_{00} being the asymptotic value of both Q and R.

The parameter d gives the rate of the evolution of R for a nonproportional loading if $A = 1$. The asymptotic values of Q and R are given by equation (32) and depend on the material parameter, g.

For a proportional loading subsequent to a non-proportional loading, equation (33) leads to a decreasing of Q from the initial value, which lies between Q_{00} and Q_0, to Q_0. A complete softening of the SH is predicted by these equations. The evolution rate is given by f. The possibilities of this new hardening rule are illustrated in Fig. 10.

Quantitative description of non-proportional effects

The above modifications of the classical models of plasticity and viscoplasticity are applied to the description of a very complext test. The complete history of the imposed straining is depicted in Fig. 11(a) and includes a sequence of increasing non-proportionalities, then a pure tension straining followed by a pure torsion loading. These two last strainings are designed so that hardening recovery and cross-hardening effects take place. Table 2 gives the parameters

Table 2 Material parameters

Models: Classical, Model 1, and Model 2	$E = 180\,000$ MPa
	$\nu = 0.33$
	$k = 114$ MPa
	$K = 92$
	$n = 8.0$
	$c = 572$
	$a = 106$
	$\phi_\infty = 0.66$
	$\varpi = 10$
	$b = 32$
	$Q = 0$
Additionally	
Model 1	$Z = 120\,000$
Model 2	$d = 16$
	$f = 0.85$
	$g = 0.1$
	$Q_0 = 0$ MPa
	$Q_\infty = 240$ MPa

used for the simulations for all the models. Figure 11(b) shows once again the deficiencies of the classical model response. It also compares the response of model 1 to experimental data. We can see that this model brings some improvements; however, it has some limitations. Since the isotropic hardening is saturated at the first level, the steady states corresponding to the subsequent levels are reached at the first cycle. The maximum equivalent stress is not obtained for the out-of-phase straining ($\varrho = 1$ and $\varphi = 90$ degrees), but for $\varphi =$ 45 degrees and $\varrho = 1$. We also observed that the recovery of the hardening is complete and instantaneous. Better results could be achieved by using a more realistic elastic domain equation such as the one studied in reference (**17**). Finally, Fig. 11(c) shows the comparison between experiment and the response of model 2. We can observe that the agreement is very satisfactory. Qualitatively, the simulations are excellent and all the non-proportional effects are described. Quantitatively, the response is also very good except in the recovery part of the test. This can be explained by the fact that the model predicts complete fading of the hardening, whereas the experimental data seem to show that there remains a permanent supplementary hardening. This can be introduced in the model with minor changes.

Conclusions

This paper is an attempt to review the effect of nonproportional loading in plasticity. A careful analysis of tests performed at ONERA and LMT/CACHAN permits a relationship between the so-called 'cross-hardening

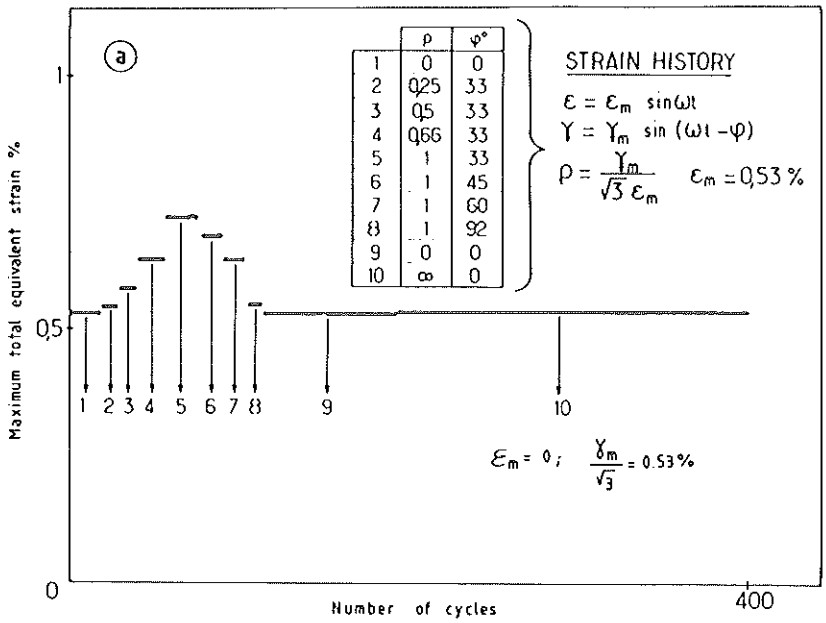

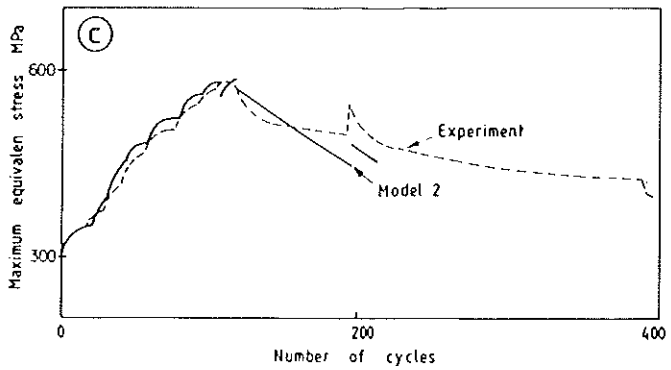

Fig 11 Simulation of a complex test and comparison with experimental data: (a) imposed strain history, (b) classical model and model 1, (c) model 2

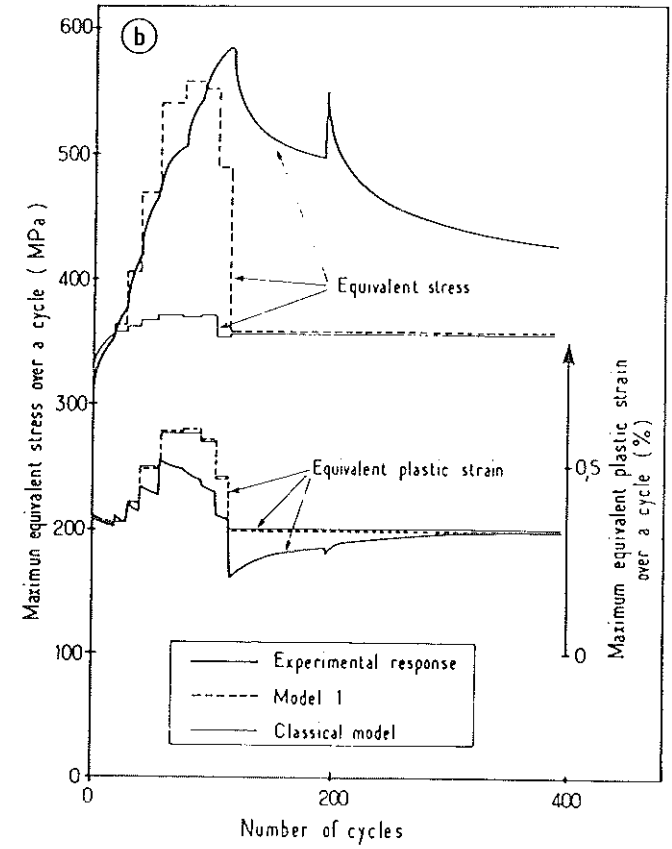
b
600
500
400
300
200
100
0
0
200
400
Number of cycles
Maximun equivalent stress over a cycle (MPa)
Equivalent stress
Equivalent plastic strain
0,5
0
Maximum equivalent plastic strain over a cycle (%)
Experimental response
Model 1
Classical model

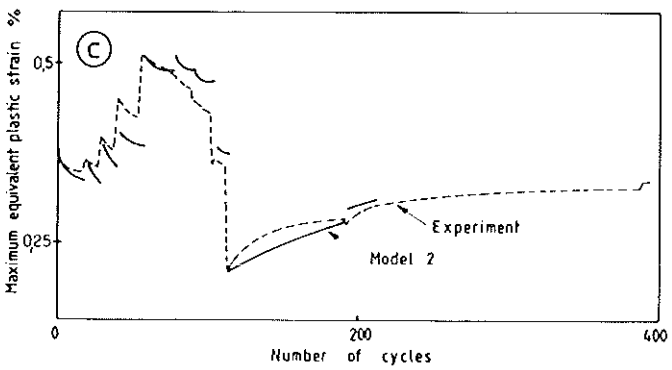
C
0,5
0,25
0
200
400
Number of cycles
Maximum equivalent plastic strain %
Experiment
Model 2

effect', that arises when the strain direction changes, to the supplementary hardening (SH) included by out-of-phase loading. Both phenomena are the mechanical expression of successive activation of different slip systems during non-proportional loading. For the aluminium alloy studied, a deformation of the elastic domain is noted, but the major effect is the increase of its size. It is the reason why, between the two modifications of the classical formulation of plasticity, the better one seems to be the modification of the isotropic hardening rule. Some points of the work require additional research; for instance, other scalar products characterizing the non-proportionality could be chosen. Other methods could be used to introduce a coupling between the non-proportionality variable and the radius of the elastic domain.

On the other hand, different materials should be tested. Up to now, multiaxial experiments have been preferentially performed on alloys with a FCC microstructure. Supplementary hardening is substantial in austenitic stainless steels and copper, but it is very low for alloys like INCO 718 (unpublished ONERA data). The response of iron (BCC), zinc or titanium alloys (HCP) is now needed to reach a better understanding of the mechanical phenomena.

Finally, we have to note that future studies on nonproportional loading have to focus on the low phase difference domain for two reasons. First, in this domain, high SH is present, and secondly, such straining paths are currently found in industrial components.

References

(1) JACKSON, P. J. and BASINSKI, J. S. (1967) Latent hardening and the flow stress in copper single crystals, *Can. J. Phys*, **45**, 707–735.
(2) FRANCIOSI, P., BERVEILLER, M., and ZAOUI, A. (1980) Latent hardening in copper and aluminium single crystals, *Acta Met.*, **28**, 273.
(3) FRANCIOSI, P. (1985) Concepts of latent and strain hardening, *Acta Met.*, **33**, 1601–1612.
(4) MANDEL, J. (1965) Généralisation de la théorie de plasticité de W. J. Koiter, *Int. J. Solids*, **1**, 273.
(5) LAMBA, H. S. and SIDEBOTTOM, O. M. (1978) Cyclic plasticity for nonproportional paths, *J. Engng Mater. Technol.*, **100**, 96–103.
(6) KANAZAWA, K., MILLER, K. J., and BROWN, M. W. (1979) Cyclic deformation of 1% Cr Mo V steel under out-of-phase loads, *Fatigue Engng Mater. Structures*, **2**, 217–228.
(7) OHASHI, Y., KAWAI, M., and KAITO, T. (1985) Inelastic behaviour of type 316 stainless steel under multiaxial nonproportional cyclic stressings at elevated temperature, *J. Engng Mater. and Technol.*, **107**, 101–109.
(8) McDOWELL, D. L. and SOCIE, D. F. (1985) Transient and stable deformation behaviour under cyclic nonproportional loadings, *ASTM-STP 853, Proceedings of the International Symposium on Biaxial–Multiaxial Fatigue*, USA, pp. 64–87.
(9) KREMPL, E. and LU, H. (1984) The hardening and rate dependent behaviour of fully annealed AISI type 304 stainless steel under biaxial in-phase and out-of-phase strain cycling at room temperature, *J. Engng Mater. Technol.*, **106**, 376–382.
(10) CAILLETAUD, G., KACZMAREK, H., and POLICELLA, H. (1984) Some elements on multiaxial behaviour of 316 stainless steel at room temperature, *Mech. Mater.*, **3**, 333–347.
(11) BENALLAL, A., LEMAITRE, J., MARQUIS, D., and ROUSSET, M. (1985) Non-proportional loading in plasticity and viscoplasticity: experimentation and modelling, *Proceedings of the Int. Conf. on Non Linear Mechanics*, Shanghai, China, pp. 438–443.

(12) NOUAILHAS, D., CHABOCHE, J. L., SAVALLE, S., and CAILLETAUD, G. (1984) On the constitutive equations for cyclic plasticity under nonproportional loadings, *Int. J. Plasticity*, **1**, 317–330.

(13) TANAKA, E., MURAKAMI, S., and OOKA, M. (1986) Effects on strain path shapes on nonproportional cyclic plasticity, *J. Mech. Phys Solids*, **33**, 559–575.

(14) CHABOCHE, J. L., DANG VAN, K., and CORDIER, G. (1979) Modelisation of the strain memory effect on the cyclic hardening of 316 stainless steel, SMIRT 5, Division L, Berlin, West Germany, paper L11/3.

(15) CAILLETAUD, G. and CHABOCHE, J. L. (1979) Macroscopic description of the microstructural changes induced by varying temperature: example of IN 100 cyclic behaviour, *Proceedings of the 3rd I.C.M.*, Cambridge, UK, Vol. 2, pp. 23–32.

(16) NOUAILHAS, D., POLICELLA, M., and KACZMAREK, M. (1983) On the description of cyclic hardening under complex loading histories, *Proceedings of International Conference on Constitutive Laws for Engineering Materials*, Edited by DESAI, C. S. and GALLAGHER, R. H., Tucson, AZ, USA, pp. 45–49.

(17) ROUSSET, M. and MARQUIS, D. (1985) Sur la déformation des surfaces seuils en plasticité cyclique, *Compte-rendu Acad. Sci. Paris, Sér. II*, **301**, 51–754.

(18) BALTOV, A. and SAWCZUK, A. (1965) A rule of anisotropic hardening, *Acta Mech.*, **1**, 1–81.